Supporting Information

Hydrodynamic interactions in squirmer dumbbells: active stress-induced alignment and locomotion

Judit Clopés, Gerhard Gompper, and Roland G. Winkler
Theoretical Physics of Living Matter, Institute of Biological Information Processing and Institute for Advanced Simulation, Forschungszentrum Jülich and JARA, 52425 Jülich, Germany

S-I. MULTIPARTICLE COLLISION DYNAMICS

In MPC, the fluid is represented by N point particles of mass m undergoing subsequent streaming and collision steps [1–4]. In the absence of any external force, the particles move ballistically in the streaming step, and their positions $\boldsymbol{r}_i(t)$ ($i \in \{1,\ldots,N\}$) are update according to

$$\boldsymbol{r}_i(t+h) = \boldsymbol{r}_i(t) + h\boldsymbol{v}_i(t), \tag{S-1}$$

where $\boldsymbol{v}_i$ is the velocity and h the time interval between collisions, which is denoted as collision time. In the collision step, the particles interact in a stochastic, but momentum conserving manner. For this purpose, the available volume is divided into cubic cells of side length a, which defines the collision environment. In the Stochastic Rotation Dynamics (SRD) version of MPC (MPC-SRD) [3], the relative velocities, with respect to the center-of-mass velocity of each cell, of the fluid particles are rotated around a randomly oriented axis by a fixed angle α. The orientation of the rotation axis is chosen randomly for every collision cell and time step. Applying the angular momentum conserving rotation (MPC-SRD+a) [5–7], the velocities after rotation are given by

$$\boldsymbol{v}_i(t+h) = \boldsymbol{v}_{cm}(t) + \mathbf{R}(\alpha)\boldsymbol{v}_{i,c} + \boldsymbol{\omega}(t)\times\boldsymbol{r}_{i,c}(t). \tag{S-2}$$

Here, the center-of-mass position and velocity are

$$\boldsymbol{r}_{cm} = \frac{1}{N_c}\sum_{i=1}^{N_c}\boldsymbol{r}_i, \qquad \boldsymbol{v}_{cm} = \frac{1}{N_c}\sum_{i=1}^{N_c}\boldsymbol{v}_i, \tag{S-3}$$

and the angular velocity is

$$\boldsymbol{\omega} = m\mathbf{I}^{-1}\sum_{j=1}^{N_c}\left\{\boldsymbol{r}_{j,c}\times(\boldsymbol{v}_{j,c} - \mathbf{R}(\alpha)\boldsymbol{v}_{j,c})\right\}. \tag{S-4}$$

$\mathbf{R}$ is the rotation matrix [3, 4], $\mathbf{I}$ denotes the moment-of-inertia tensor of the respective particles in the collision cell with respect to their center-of-mass, and $\boldsymbol{r}_{ic} = \boldsymbol{r}_i - \boldsymbol{r}_{cm}$, $\boldsymbol{v}_{ic} = \boldsymbol{v}_i - \boldsymbol{v}_{cm}$. Since this rotation violates energy conservation, we apply the Maxwell-Boltzmann scaling approach, which yields a Maxwellian distribution of kinetic energy.

Discretization in collision cells implies violation of Galilean invariance. To restore Galilean invariance, a random shift of the entire computational grid is applied [8, 9].

S-II. RIGID BODY DYNAMICS OF SPHEROIDS

This section describes a general procedure for the solution of the rigid body equations of motion of spheroidal colloids with spheres as a special case.

During the MPC streaming step, a spheroid moves according to rigid-body dynamics, i.e., translational motion for the center of mass position, $\boldsymbol{C}$, and rotation, which is described by a quaternion, $\boldsymbol{q} = (q_0, q_1, q_2, q_3)^T$ [13], as described in Ref. [14]. Explicitly, the equations of motion are given by

$$M\ddot{\boldsymbol{C}} = \boldsymbol{F}, \tag{S-5}$$

$$\ddot{\boldsymbol{q}} = \frac{1}{2}\left[\boldsymbol{Q}(\dot{\boldsymbol{q}})\begin{pmatrix}0\\ \boldsymbol{\Omega}^b\end{pmatrix} + \boldsymbol{Q}(\boldsymbol{q})\begin{pmatrix}0\\ \dot{\boldsymbol{\Omega}}^b\end{pmatrix}\right], \tag{S-6}$$

$$\dot{\boldsymbol{q}} = \frac{1}{2}\boldsymbol{Q}(\boldsymbol{q})\begin{pmatrix}0\\ \boldsymbol{\Omega}^b\end{pmatrix}, \tag{S-7}$$

$$\frac{d\Omega^b_\alpha}{dt} = I_\alpha^{-1}\left[T^b_\alpha + (I_\beta - I_\gamma)\Omega^b_\beta\Omega^b_\gamma\right]. \tag{S-8}$$

Here, $\boldsymbol{Q}(\boldsymbol{q})$ is

$$\boldsymbol{Q}(\boldsymbol{q}) = \begin{pmatrix} q_0 & -q_1 & -q_2 & -q_3\\ q_1 & q_0 & -q_3 & q_2\\ q_2 & q_3 & q_0 & -q_1\\ q_3 & -q_2 & q_1 & q_0\end{pmatrix} \tag{S-9}$$

and $\boldsymbol{F}$ and $\boldsymbol{T}$ are the force and torque acting on the spheroid. Forces and torques are derived from steric interactions with another squirmers. Equations (S-8) are Euler's equations for rigid body dynamics and hold for $(\alpha,\beta,\gamma) = (x,y,z)$, (y,z,x), and (z,x,y). The superscript b refers to the body fixed reference frame. Body-fixed and laboratory-frame quantities can be related via

$$\boldsymbol{a}^{\mathrm{b}} = \mathbf{D}\boldsymbol{a}^{\mathrm{s}}, \tag{S-10}$$

where $\boldsymbol{a}^{\mathrm{b}}$ is a vector in the body-fixed reference frame and $\boldsymbol{a}^{\mathrm{s}}$ a vector in the laboratory frame (space fixed). The rotation matrix, $\mathbf{D}$, is related to the quaternion $\boldsymbol{q}$ by

$$\mathbf{D} = \begin{pmatrix} q_0^2+q_1^2-q_2^2-q_3^2 & 2(q_1q_2+q_0q_3) & 2(q_1q_3-q_0q_2)\\ 2(q_2q_1-q_0q_3) & q_0^2-q_1^2+q_2^2-q_3^2 & 2(q_2q_3+q_0q_1)\\ 2(q_2q_1+q_0q_2) & 2(q_3q_2-q_0q_1) & q_0^2-q_1^2-q_2^2+q_3^2\end{pmatrix}.$$

The orientation vector of a spheroid is $\boldsymbol{e}^{\mathrm{s}} = \mathbf{D}^T\boldsymbol{e}^{\mathrm{b}} = \mathbf{D}^T(0,0,1)^T$. The moment of inertia tensor in the body-fixed frame $\mathbf{I}^b$ is a constant diagonal matrix with diagonal

elements $I_x = (M/5)(b_x^2 + b_z^2) = I_y$ and $I_z = (2M/5)b_x^2$. When needed, the angular velocity is calculated as $\boldsymbol{\Omega}^{\mathrm{s}} = \mathbf{D}^T \left(\mathbf{I}^{\mathrm{b}}\right)^{-1} \mathbf{D}\boldsymbol{L}^{\mathrm{s}}$, where $\boldsymbol{L}^{\mathrm{s}}$ is the angular momentum. For vectors in the laboratory frame, we will frequently omit the superscript.

For the numerical integration of the equations of motion, the Verlet algorithm for rigid-body rotational motion is applied, as proposed in Ref. [13]. Integration for a time step τ is performed as follows:

- Update $\boldsymbol{C}$ and $\boldsymbol{q}$ according to

$$\boldsymbol{C}(t+\tau) = \boldsymbol{C}(t) + \boldsymbol{U}(t)\tau + \frac{\tau^2}{2M}\boldsymbol{F}^s(t), \tag{S-11}$$

$$\boldsymbol{q}(t+\tau) = (1-\tilde{\lambda})\boldsymbol{q}(t) + \dot{\boldsymbol{q}}\tau + \frac{\tau^2}{2}\ddot{\boldsymbol{q}}, \tag{S-12}$$

$$\tilde{\lambda} = 1 - \dot{\boldsymbol{q}}^2\tau^2/2 - \sqrt{1 - \dot{\boldsymbol{q}}^2\tau^2 - \dot{\boldsymbol{q}}\cdot\ddot{\boldsymbol{q}}\tau^3 - (\ddot{\boldsymbol{q}}^2 - \dot{\boldsymbol{q}}^4)\tau^4/4}. \tag{S-13}$$

  The parameter $\tilde{\lambda}$ is introduced to ensure $\boldsymbol{q}^2 = 1$.

- Calculate forces and torques $\boldsymbol{F}^s(t+\tau)$ and $\boldsymbol{T}^s(t+\tau)$.

- Update $\boldsymbol{U}$ and $\boldsymbol{L}^s$ according to

$$\boldsymbol{U}(t+\tau) = \boldsymbol{U}(t) + \frac{\tau}{2M}[\boldsymbol{F}^s(t) + \boldsymbol{F}^s(t+\tau)], \tag{S-14}$$

$$\boldsymbol{L}^{\mathrm{s}}(t+\tau) = \boldsymbol{L}^{\mathrm{s}}(t) + \frac{\tau}{2}[\boldsymbol{T}^{\mathrm{s}}(t) + \boldsymbol{T}^{\mathrm{s}}(t+\tau)]. \tag{S-15}$$

S-III. IMPLEMENTATION OF A SPHEROIDAL SQUIRMER IN MPC

A. Streaming step

During the streaming step, a spheroid will collide with several MPC particles. Since the total change in (angular) momentum of a spheroid in a streaming step is small, we perform the collisions with MPC particles in a coarse-grained way [15] (see also Ref. [16]).

At first, we perform a streaming from t to $t+h$ without interactions with MPC particles, but taking steric interactions into account as described in Sec. S-II. Subsequently, all MPC particles are streamed, i.e., their positions are updated as described in Sec. S-I, where a certain fraction of MPC particles penetrates a spheroid. Each particle i inside a spheroid at time $t+h$ is moved back in time by half a time step and subsequently translated onto the spheroid's surface. The translation can be realized in different ways. One possibility is to construct a virtual spheroid with semi-axes $\tilde{b}_z$, $\tilde{b}_x$, $\tilde{b}_z/\tilde{b}_x = b_z/b_x$ and $\boldsymbol{r}_i(t+h/2)$ on its surface. The particle is then translated along the normal vector of the virtual spheroid until it is on the real spheroid's surface. Alternatively, the difference vector $\boldsymbol{r}_i(t+h/2) - \boldsymbol{C}(t+h/2)$ can be scaled such that the particle position lies on the spheroid's surface. A comparison yields no significant difference. For all MPC particle on the spheroid's surface at $t+h/2$, the momentum transfer

$$\boldsymbol{J}_i = 2m\left\{\boldsymbol{v}_i - \boldsymbol{U} - \boldsymbol{\Omega}\times(\boldsymbol{r}_i - \boldsymbol{C}) - \mathbf{D}^T\boldsymbol{u}_{sq}^{\mathrm{b}}[\mathbf{D}(\boldsymbol{r}_i - \boldsymbol{C})]\right\} \tag{S-16}$$

is determined, taking into account the squirmer surface fluid velocity $\boldsymbol{u}_{sq}$ of Eq. (1) [17]. A useful identity to determine the tangent vector $\boldsymbol{s}$ on the squirmer surface is given in Eq. (8) of Ref. [18], and the coordinate ζ is given by

$$\zeta = \frac{1}{2c}\left(\sqrt{x^2+y^2+(z+c)^2} - \sqrt{x^2+y^2+(z-c)^2}\right). \tag{S-17}$$

The velocity of the MPC particle is updated according to $\boldsymbol{v}_i' = \boldsymbol{v}_i - \boldsymbol{J}_i/m$. Subsequently, the position $\boldsymbol{r}_i(t+h)$ is obtained by streaming the MPC particle for the remaining time $h/2$ with velocity $\boldsymbol{v}_i'$, i.e., $\boldsymbol{r}_i(t+h) = \boldsymbol{r}_i(t+h/2) + h\boldsymbol{v}_i'/2$.

As a consequence of the elastic collisions, the center-of-mass velocity and rotation frequency of a spheroid are finally given by

$$\boldsymbol{U}(t+h) = \boldsymbol{U}'(t+h) + \boldsymbol{J}/M, \tag{S-18}$$

$$\boldsymbol{\Omega}(t+h) = \boldsymbol{\Omega}'(t+h) + \boldsymbol{D}^T\left(\boldsymbol{I}^b\right)^{-1}\boldsymbol{D}\boldsymbol{L}, \tag{S-19}$$

where $\boldsymbol{J} = \sum_i \boldsymbol{J}_i$ is total momentum transfer by the MPC fluid and $\boldsymbol{L} = \sum_i (\boldsymbol{r}_i(t+h/2) - \boldsymbol{C}(t+h/2)) \times \boldsymbol{J}_i$ is the respective angular momentum transfer. The prime indicates the velocity and rotation frequency after streaming without MPC interactions.

B. Collision step

For the collision step with MPC particles, phantom particles are distributed inside each spheroid for no-slip boundary conditions [8, 15, 16]. Their number density and mass are equal to those of fluid particles. Phantom particle positions $\boldsymbol{r}_i^p$ are uniformly distributed inside a spheroid and their velocities are given by

$$\boldsymbol{v}_i^p = \boldsymbol{U} + \boldsymbol{\Omega}\times(\boldsymbol{r}_i - \boldsymbol{C}) + \boldsymbol{u}_{sq,i} + \boldsymbol{v}_i^R. \tag{S-20}$$

The Cartesian components of $\boldsymbol{v}_i^R$ are Gaussian-distributed random numbers with zero mean and variance $\sqrt{k_BT/m}$. The squirming velocity $\boldsymbol{u}_{sq,i}$ is determined by Eq. (1) of the main document, with the phantom particle position projecting onto the spheroid's surface (cf. Sec. S-III A). As a result of MPC collisions, a spheroid's linear and angular momenta change by $\boldsymbol{J}_i^p = m(\bar{\boldsymbol{v}}_i^p - \boldsymbol{v}_i^p)$ and $\boldsymbol{L}_i^p = (\boldsymbol{r}_i^p - \boldsymbol{C}) \times \boldsymbol{J}_i^p$, where $\bar{\boldsymbol{v}}_i^p$ and $\boldsymbol{v}_i^p$ are the phantom particle's velocity after and before the MPC collision. Hence, the spheroid velocity and angular velocity become

$$\boldsymbol{U}(t+h) = \boldsymbol{U}(t+h) + \boldsymbol{J}^p(t+h)/M, \tag{S-21}$$

$$\boldsymbol{\Omega}(t+h) = \boldsymbol{\Omega}(t+h) + \mathrm{R}^T\left(\mathbf{I}^{\mathrm{b}}\right)^{-1}\mathrm{R}\boldsymbol{L}^p. \tag{S-22}$$

Here, $\boldsymbol{U}(t+h)$ and $\boldsymbol{\Omega}(t+h)$ on the right-hand side are the values after streaming, Eq. (S-18) and (S-19).

S-IV. STERIC INTERACTIONS

Excluded-volume interactions between spheroids are taken into account by the approach provided in Ref. [19], see also [16].

The spheroid's surface in the laboratory frame is given by the quadratic form

$$1 = \mathcal{A}(\boldsymbol{x}) \equiv (\boldsymbol{x} - \boldsymbol{C})^T \boldsymbol{A} (\boldsymbol{x} - \boldsymbol{C}), \tag{S-23}$$

where the orientation matrix $\boldsymbol{A}$ can be expressed as

$$\boldsymbol{A} = (\boldsymbol{1} - \boldsymbol{e}\boldsymbol{e}^T)/b_x^2 + \boldsymbol{e}\boldsymbol{e}^T/b_z^2; \tag{S-24}$$

$\boldsymbol{1}$ is the unit matrix. For the steric interactions, we introduce a virtual safety distance d_v, which is small compared to b_x and b_z. When computing steric interactions, we replace b_x and b_z by $b_x + d_v$ and $b_z + d_v$, respectively. For all simulations, the value $d_v = 0.7a$ is used.

The potential

$$U = 4\epsilon_0 \left[\left(\frac{\sigma_0}{d_R + \sigma_0} \right)^{12} - \left(\frac{\sigma_0}{d_R + \sigma_0} \right)^{6} \right] \tag{S-25}$$

between spheroids is introduced to prevent their overlap. Here, σ_0 and ϵ_0 correspond to a length and energy scale, respectively, which are set to $\epsilon_0 = k_B T$ and $\sigma_0 = 2d_v$. The directional contact distance d_R between two spheroids, with orientation matrices $\boldsymbol{A}_1$, $\boldsymbol{A}_2$ and center positions $\boldsymbol{C}_1$, $\boldsymbol{C}_2$, is an approximation to their true distance of closest approach and is defined by

$$d_R = R(1 - F(\boldsymbol{A}_1, \boldsymbol{A}_2)^{-1/2}) \tag{S-26}$$

Here, $\boldsymbol{R} = \boldsymbol{C}_2 - \boldsymbol{C}_1$, $R = |\boldsymbol{R}|$, and $F(\boldsymbol{A}_1, \boldsymbol{A}_2)$ is the elliptic contact function, defined as [19]

$$\begin{aligned} F(\boldsymbol{A}_1, \boldsymbol{A}_2) &= \max_{\lambda} \min_{\boldsymbol{x}} \mathcal{S}(\boldsymbol{x}, \lambda) \\ &= \max_{\lambda} \min_{\boldsymbol{x}} \left(\lambda \mathcal{A}_1(\boldsymbol{x}) + (1 - \lambda) \mathcal{A}_2(\boldsymbol{x}) \right). \end{aligned} \tag{S-27}$$

Minimization with respect to $\boldsymbol{x}$ demands $\boldsymbol{\nabla} \mathcal{S}(\boldsymbol{x}, \lambda) = 0$, and hence,

$$\boldsymbol{x}(\lambda) = \left\{ \lambda \boldsymbol{A}_1 + (1 - \lambda) \boldsymbol{A}_2 \right\}^{-1} \left\{ \lambda \boldsymbol{A}_1 \boldsymbol{C}_1 + (1 - \lambda) \boldsymbol{A}_2 \boldsymbol{C}_2 \right\}. \tag{S-28}$$

The value $\lambda = \lambda_c$ that maximizes $\mathcal{S}(\boldsymbol{x}(\lambda), \lambda)$ can be found by the root finding problem

$$\mathcal{A}_1(\boldsymbol{x}(\lambda)) - \mathcal{A}_2(\boldsymbol{x}(\lambda)) = 0. \tag{S-29}$$

The forces and torques arising from the potential (S-25) can be calculated analytically and are given by [19]

$$\begin{aligned} \boldsymbol{F}_1 =& \frac{24\epsilon_0}{\sigma_0} \left[2 \left(\frac{\sigma_0}{d_R + \sigma_0} \right)^{13} - \left(\frac{\sigma_0}{d_R + \sigma_0} \right)^{7} \right] \\ & \times \left(\frac{\boldsymbol{R}}{R} (F^{-1/2} - 1) - \frac{R}{2} F^{-3/2} \boldsymbol{X}_c \right), \end{aligned} \tag{S-30}$$

and

$$\boldsymbol{T}_1 = - \frac{12R\epsilon_0}{\sigma_0} \left[2 \left(\frac{\sigma_0}{d_R + \sigma_0} \right)^{13} - \left(\frac{\sigma_0}{d_R + \sigma_0} \right)^{7} \right] \tag{S-31}$$

$$\times F^{-3/2} (\boldsymbol{x}_c - \boldsymbol{C}) \times \boldsymbol{X}_c \tag{S-32}$$

for the first spheroid, where $\boldsymbol{X}_c = 2\lambda_c \boldsymbol{A}_1 (\boldsymbol{x}_c - \boldsymbol{C}_1)$. The force and torque on the second spheroid follow by Newton's action-reaction law, i.e.,

$$\boldsymbol{F}_2 = -\boldsymbol{F}_1, \tag{S-33}$$

$$\boldsymbol{T}_2 = -\boldsymbol{T}_1 + \boldsymbol{R} \times \boldsymbol{F}_1. \tag{S-34}$$

We restrict ourselves to short-rang repulsive interactions by setting the potential U to a constant value for $d_R > (\sqrt[6]{2} - 1)\sigma_0$, which implies that $\boldsymbol{F}_1$ and $\boldsymbol{T}_1$ are zero for this range of d_R values. Note that an upper bound to d_R is $R - 2b_z$, which means that two spheroids will not interact if $R > 2b_z + (\sqrt[6]{2} - 1)\sigma_0$. This inequality is checked before a numerical calculation of d_R is employed.

S-V. DECAY TIME OF THE BOND-VECTOR AUTOCORRELATION FUNCTION

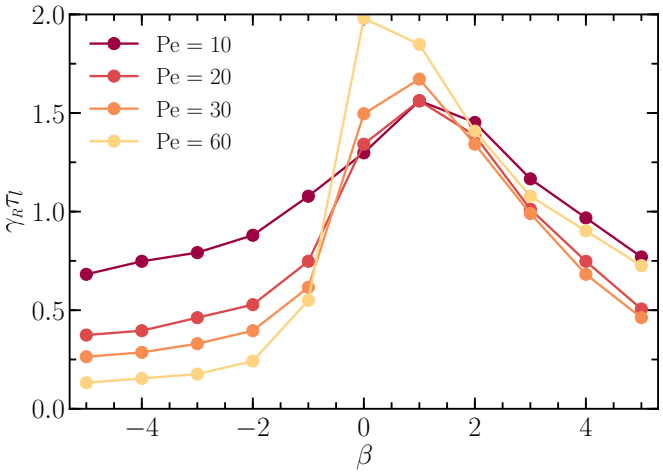

FIG. S1. Characteristic decay time τ_l of the bond-vector orientational autocorrelation function of Fig. 7 as a function of the active stress β for the Péclet numbers Pe = 10, 20, 30, and 60. The decay time is scaled by the rotational diffusion coefficient of a passive colloid, where $\gamma_R = 2D_R^0$.

S-VI. CORRELATION FUNCTION OF PROPULSION DIRECTION AND BOND VECTOR

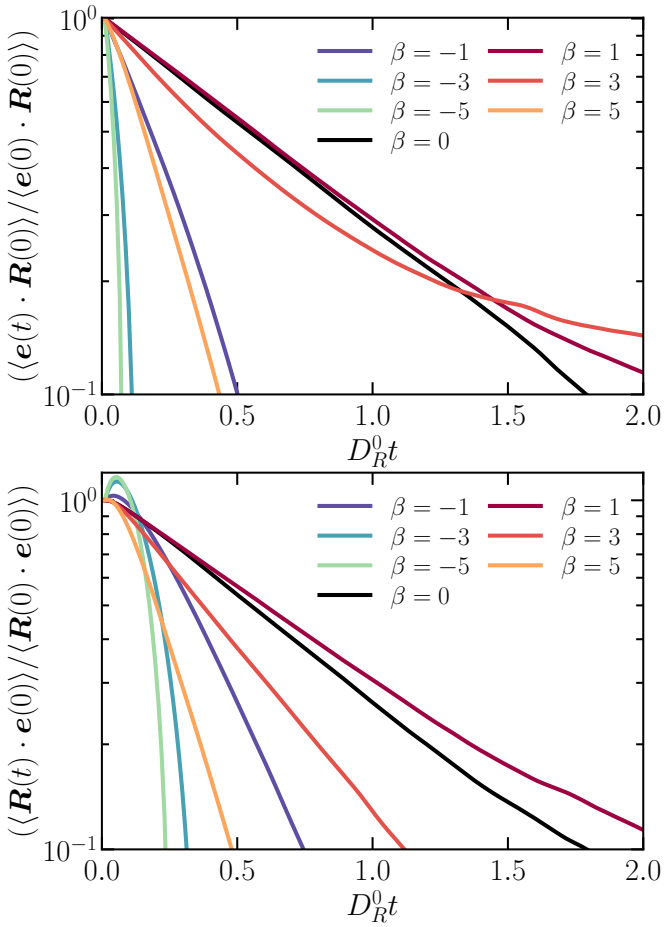

FIG. S2. (Top) Correlation function of the squirmers propulsion direction, $\boldsymbol{e}(t)$ and the bond vector $\boldsymbol{R}$. (Bottom) Correlation function the bond vector and the squirmers propulsion direction. The Péclet number is Pe = 30. The two correlations show qualitative and quantitative differences reflecting the complexity of the strong hydrodynamic coupling between the two squirmers of the dumbbell.

S-VII. SQUIRMER-SQUIRMER PROPULSION ALIGNMENT

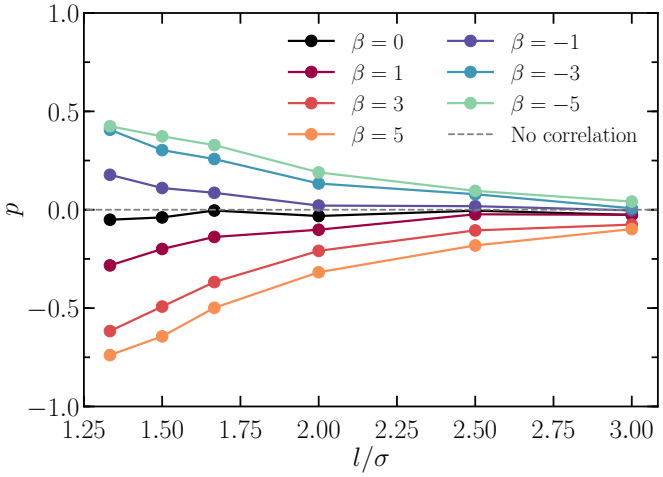

FIG. S3. Average alignment $p = \langle \boldsymbol{e}_1 \cdot \boldsymbol{e}_2 \rangle$ of the squirmer propulsion directions as a function of the dumbbell bond length for the active stress $\beta = 0$, ± 1, ± 3, and ± 5. The Péclet number is $Pe = 10$.

S-VIII. BOND FORCE

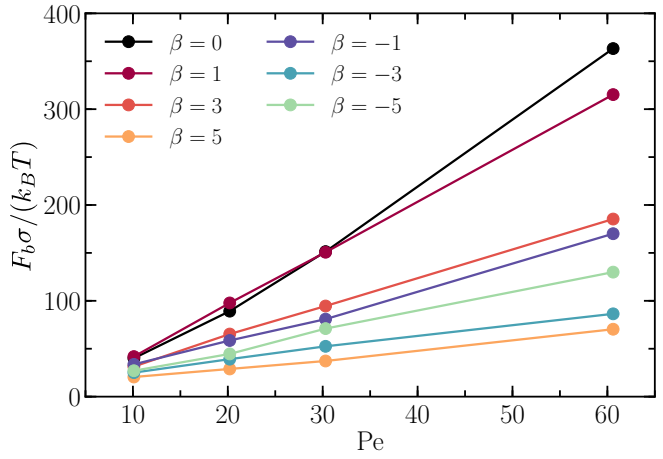

FIG. S4. Bond force (Eq. (13)) as a function of Péclet number for the indicated active stresses.

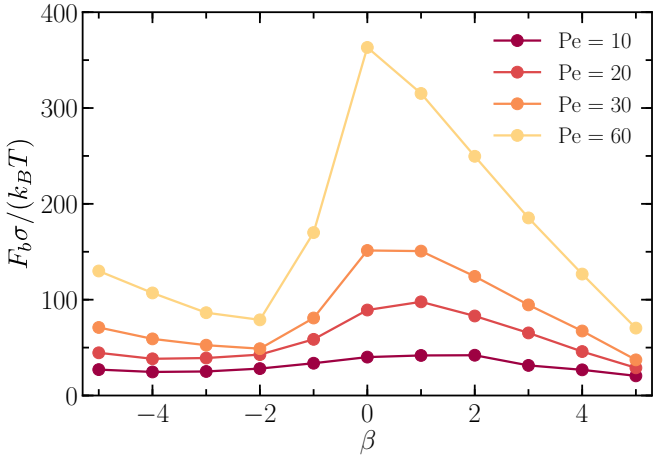

FIG. S5. Bond force (Eq. (13)) as a function of β for the indicated Péclet numbers.

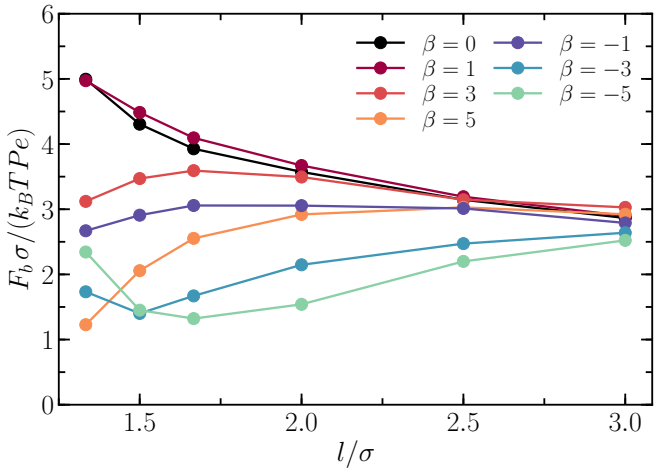

FIG. S6. Bond force (Eq. (13)) as a function of the dumbbell bond length for the indicated active stress and $Pe = 30$.

S-IX. MEAN-SQUARE DISPLACEMENT

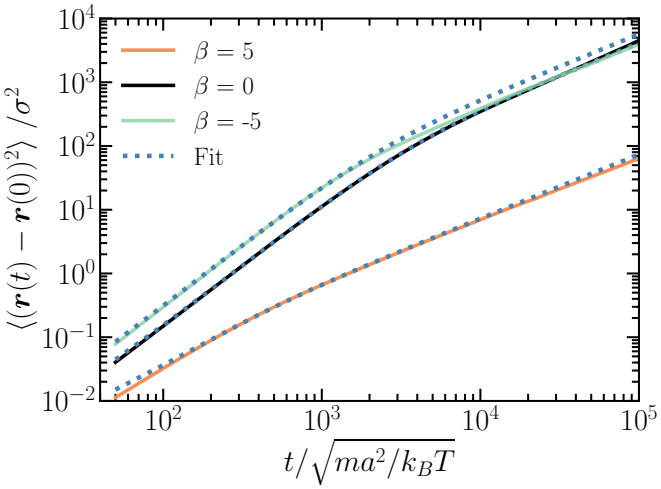

FIG. S7. Center-of-mass mean-square displacement of squirmer dumbbells as a function of the scaled time $D_R^0 t$ for the indicated active stresses and the Péclet number $Pe = 30$. The dotted lines are fits with the MSD of active Brownian dumbbells, Eq. (14).

S-X. MOVIES

- **Movie M1:** M1_Beta-5CM.mpeg
  Squirmer dumbbell in the center-of-mass reference frame: $Pe = 30$ and $\beta = -5$ (pusher).
- **Movie M2:** M2_Beta-5lab.mpeg
  Squirmer dumbbell in the laboratory reference frame: $Pe = 30$ and $\beta = -5$ (pusher).
- **Movie M3:** M3_Beta5CM.mpeg
  Squirmer dumbbell in the center-of-mass reference frame: $Pe = 30$ and $\beta = 5$ (puller).
- **Movie M4:** M4_Beta5lab.mpeg
  Squirmer dumbbell in the laboratory reference frame: $Pe = 30$ and $\beta = 5$ (puller).

[1] A. Malevanets and R. Kapral, Mesoscopic model for solvent dynamics, J. Chem. Phys. **110**, 8605 (1999).

[2] R. Kapral, Multiparticle collision dynamics: Simulations of complex systems on mesoscale, Adv. Chem. Phys. **140**, 89 (2008).

[3] G. Gompper, T. Ihle, D. M. Kroll, and R. G. Winkler, Multi-particle collision dynamics: A particle-based mesoscale simulation approach to the hydrodynamics of complex fluids, Adv. Polym. Sci. **221**, 1 (2009).

[4] R. G. Winkler, Flow simulations with multiparticle collision dynamics, in *Hierarchical Methods for Dynamics in Complex Molecular Systems*, IAS Series, Vol. 10, edited by J. Grotendorst, G. Sutmann, G. Gompper, and D. Marx (Forschungszentrum Jülich GmbH, Jülich, 2012).

[5] H. Noguchi and G. Gompper, Transport coefficients of off-lattice mesoscale-hydrodynamics simulation techniques, Phys. Rev. E **78**, 016706 (2008).

[6] M. Theers and R. G. Winkler, Bulk viscosity of multiparticle collision dynamics fluids, Phys. Rev. E **91**, 033309 (2015).

[7] M. Yang, M. Theers, J. Hu, G. Gompper, R. G. Winkler, and M. Ripoll, Effect of angular momentum conservation on hydrodynamic simulations of colloids, Phys. Rev. E **92**, 013301 (2015).

[8] A. Lamura, G. Gompper, T. Ihle, and D. M. Kroll, Multiparticle collision dynamics: Flow around a circular and a square cylinder, Europhys. Lett. **56**, 319 (2001).

[9] T. Ihle and D. M. Kroll, Stochastic rotation dynamics: A Galilean-invariant mesoscopic model for fluid flow, Phys. Rev. E **63**, 020201(R) (2001).

[10] R. G. Winkler and C.-C. Huang, Stress tensors of multiparticle collision dynamics fluids, J. Chem. Phys. **130**, 074907 (2009).

[11] C.-C. Huang, A. Chatterji, G. Sutmann, G. Gompper, and R. G. Winkler, Cell-level canonical sampling by velocity scaling for multiparticle collision dynamics simulations, J. Comput. Phys. **229**, 168 (2010).

[12] C.-C. Huang, A. Varghese, G. Gompper, and R. G. Winkler, Thermostat for nonequilibrium multiparticle-collision-dynamics simulations, Phys. Rev. E **91**, 013310 (2015).

[13] I. P. Omelyan, Algorithm for numerical integration of the rigid-body equations of motion, Phys. Rev. E **58**, 1169 (1998).

[14] M. Theers, E. Westphal, G. Gompper, and R. G. Winkler, From local to hydrodynamic friction in Brownian motion: A multiparticle collision dynamics simulation study, Phys. Rev. E **93**, 032604 (2016).

[15] J. T. Padding, A. Wysocki, H. Löwen, and A. A. Louis, Stick boundary conditions and rotational velocity autocorrelation functions for colloidal particles in a coarse-grained representation of the solvent, J. Phys.: Condens. Matter **17**, S3393 (2005).

[16] M. Theers, E. Westphal, G. Gompper, and R. G. Winkler, Modeling a spheroidal microswimmer and cooperative swimming in a narrow slit, Soft Matter **12**, 7372 (2016).

[17] M. T. Downton and H. Stark, Simulation of a model microswimmer, J. Phys.: Condens. Matter **21**, 204101 (2009).

[18] S. R. Keller and T. Y. Wu, A porous prolate-spheroidal model for ciliated micro-organisms, J. Fluid Mech. **80**, 259 (1977).

[19] L. Paramonov and S. N. Yaliraki, The directional contact distance of two ellipsoids: Coarse-grained potentials for anisotropic interactions, J. Chem. Phys. **123**, 194111 (2005).